Fermilab

Irradiation Tests of Superconducting Detectors and Comparison with Simulations

FERMILAB-PUB-20-145-AE

Fermilab Accepted Manuscript

Irradiation Tests of Superconducting Detectors and Comparison with Simulations

Y. Minami[1] · Y. Akiba[1,2] · S. Beckman[3] · M. Hazumi[1,2,4,5] · C. Kuo[6,7] ·
N. A. Kurinsky[8,9] · H. Kutsuma[10,11] · A. T. Lee[3,12] · S. Mima[11] · C. R. Raum[3] ·
T. Sasse[3] · S. L. Stever[5] · A. Suzuki[12] · B. Westbrook[3]

Abstract

For the future satellite mission at the second sun–earth Lagrangian point (L2), we need to mitigate phonon propagation created by cosmic rays to superconducting detectors. We simulate phonon propagation in silicon substrate and show that putting a metal layer on the substrate or making hole in the substrate reduces the propagation. We also show a function which shows the response of a TES bolometer on a substrate. To validate these theoretical expectations, we make irradiation tests using two types of superconducting detectors: transition edge sensor bolometers and kinetic inductance detectors. From the tests, we show that putting metal can reduce correlations between detectors and number of hit events from charged particles.

Keywords Cosmic microwave background · Transition edge sensors · Kinetic inductance detectors · Phonon

1 Introduction

We target to realise a future satellite mission, LiteBIRD [1], which will observe full sky at the second sun–earth Lagrangian point (L2) and measure the polarisation of the cosmic microwave backgrounds (CMB). We plan to use transition edge sensor (TES) bolometers [2] to measure the polarisation signal. Measurements of Planck satellite mission [3] at L2 were disturbed by cosmic rays. Therefore, we need to mitigate the effects from galactic cosmic rays to realise our mission.

Our main concern is the following process: (1) cosmic rays deposit energy in silicon substrate where bolometers are. (2) The energy is propagated by phonons in the silicon substrate. (3) When some phonons enter a bolometer, the bolometer senses it and spurious signal is created.

✉ Y. Minami
  yminami@post.kek.jp

Extended author information available on the last page of the article
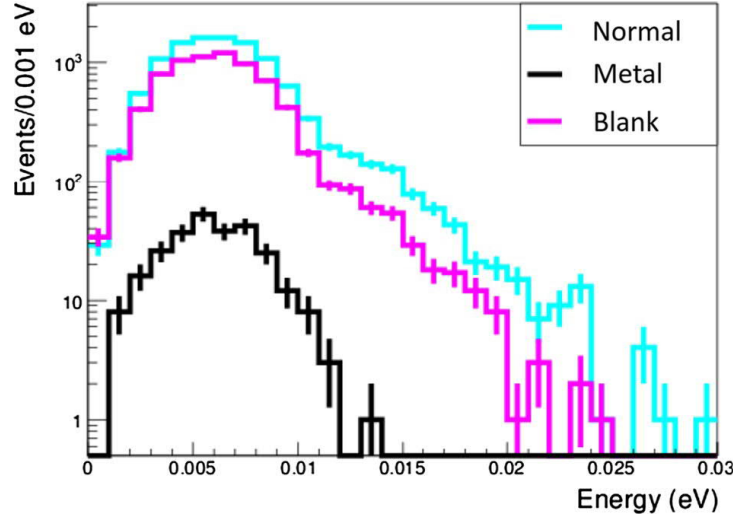
Fig. 1 Energy propagation by phonons simulated by G4CMP [4–6]. With a simple configuration, we simulate phonon propagation in silicon. We studied two methods of mitigation: (1) putting metal on a silicon to absorb phonons by electrons and (2) making a hole to disturb the phonon propagation to detectors. We also checked the case without treatment, or Control. These quick simulation results show that phonon propagation is effectively mitigated by putting metal and slightly mitigated by making a hole (Color figure online)

In our study, the phonon propagation is simulated by G4CMP [4–6]. We find that we can mitigate the phonon propagation by putting metal on silicon substrate or making holes in the silicon substrate (Fig. 1).[1]

Because phonons travel 4π directions, we can apply mitigation treatment only on the surface of substrate.

For the study of heat propagation, we model a TES bolometer as shown in Fig. 2. From this model, we find that the response of a TES bolometer against energy input by a particle is characterised with the function:

$$-Ae^{-(t-t_0)/\tau_A} + Be^{-(t-t_0)/\tau_B},\qquad(1)$$

where A and B are coefficients, and τ_A and τ_B are the time constant which consists of a signal.[2] As we explain precisely in Appendix 1, we can categorise signals into two types of events:

- $A = B$: the charged particle deposits energy in the silicon substrate.
- $A \neq B$: the charged particle deposits energy directly in the TES bolometer.

---

[1] In the simulation, we prepare block of silicon surrounded by phonon absorbing walls. Then, we generate phonons in a position and see how much phonons are propagated in the other position across the area with mitigation methods (including no mitigation). Because the simulation parameters are not optimised, we only see the relative effects of mitigation ideas.

[2] As described in Appendix 1, A is related to amplitude of rising signal, B is related to amplitude of dropping signal, τ_A is related to substrate-bath time constant, and τ_B is related to TES-substrate time constant.

Fig. 2 Thermal model of a
TES bolometer. We assume a
TES bolometer is on a silicon
substrate, which is itself on a
thermal bath. C_∞, C_1, and C_2 are
thermal capacitance of thermal
bath, silicon substrate, and
TES bolometer (respectively).
G_1 is a thermal conductivity
between the silicon substrate
and the thermal bath, and G_2 is
one between the TES bolometer
and the silicon substrate (Color
figure online)
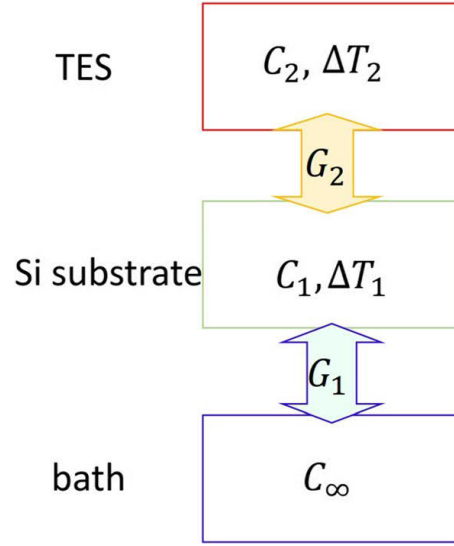
In this paper, we try to validate the simulation results and models with experiments. We irradiate superconducting detectors with α-ray source (^{241}Am) which deposit energy in silicon substrates. We test how the energy propagations by phonons are mitigated.

We prepare two types of superconducting detectors for the experiments: transition edge sensor (TES) bolometers to validate both the simulation results and model and kinetic inductance detectors (KIDs) to validate simulation results.

The rest of the paper is organised as follows: in Sect. 2, we describe the experimental set-up of the irradiation tests. In Sect. 3, we show how we analyse data and the main results. We conclude in Sect. 4.

2 Experimental Set-Up

2.1 Set-Up of TES Bolometers

We designed TES bolometers as shown in Fig. 3. We fabricated three types of bolometers: (1) putting metal on a silicon to absorb phonons by electrons; (2) making a hole to disturb the phonon propagation to detectors; and (3) control ones without mitigation ideas for the comparison.

For the readout of TES bolometers, we use almost the same readout system used in POLARBEAR-2 [9]. The different points are as follows:

- Temperature of TES bolometer stage: 300 mK
- Readout frequency : < 1.2 MHz
- Sampling rate: ~ 600 Hz

TES bolometers are AC-biased and tuned at the transition edge. Temperature change in TES bolometers is read out as bias powers to the TES bolometers.
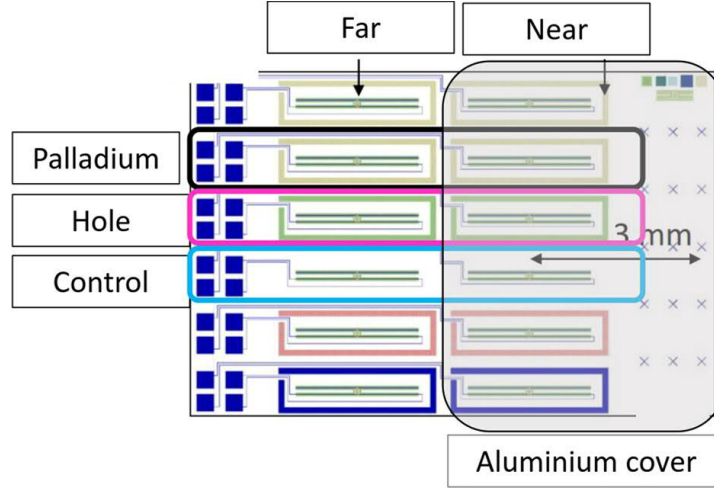
Fig. 3 Design of TES bolometers. They are on a silicon substrate whose thickness is 675 μm. We prepared three types of TES bolometers: surrounded by palladium, surrounded by a hole at the surface of the silicon substrate (depth is 30–50 μm), and control for the comparison. Details of fabrication are described in [10]. We adopt palladium because the heat capacity per volume is about ten times larger than gold and it can reduce the thickness of metal. We prepared two TESs for each design (Far/Near). One is exposed to α-ray source (Far), and the other is covered with aluminium plate (Near) which is thick enough to stop α-rays (Color figure online)

Table 1 Description of TES and readout SQUIDs

| TES name	TES id
Palladium Far	1
Control Far	2
Remove bulk silicon Far	4
Remove bulk silicon Near	6
Palladium Near	7
Control Near	8

Two TES bolometers are read out through a SQUID

Time-ordered data of bolometers are multiplexed by resonators and amplified by SQUIDs. The amplified signal is transferred to readout devices at normal temperature.

We summarise the detailed TES designs as shown in Table 1. From our fabrication set-up, we estimate $\tau_B \sim 10$ms.

2.2 Set-Up of KIDs

We designed KIDs as shown in Fig. 4. We make a hole and put gold on the silicon. Because of difference of fabrication facilities, we adopt gold as normal metal on the contrary to the TES chip. Ten KIDs with different resonant frequencies are designed to be on one silicon substrate. Ten different resonances around 5.43 GHz are allocated with ascending order from f1 to f10. Readout system of KIDs is summarised in Fig. 5 and Table. 2.
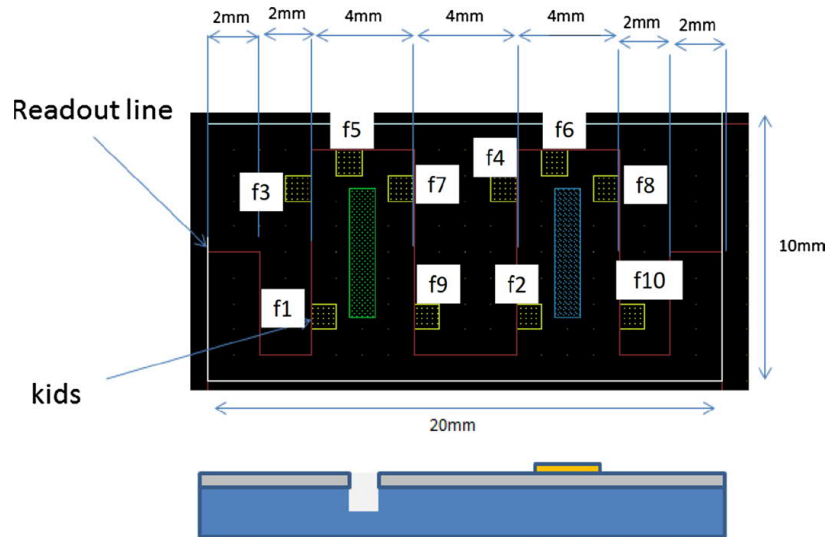
Fig. 4 Design of KIDs. We put ten KIDs (from f1 to f10) in one readout line. Green meshed area surrounded by f1, f3, f5, f7, and f9 shows the bulk silicon is removed. Blue meshed area surrounded by f2, f4, f6, f8, and f10 shows gold is on (Color figure online)

Fig. 5 17 dBm of 5.43 GHz signal is generated by local oscillator (LO) and modulated with 200 MHz signal with IQ mixer. The modulated signal is propagated to KIDs through coaxial cables. The estimated power input to KIDs is about -65.5 dB. After the KIDs, signals are amplified with HEMT amplifier in 4 K and three amplifiers in 300 K. Then, the signal is demodulated and digitised data are read [7, 8]
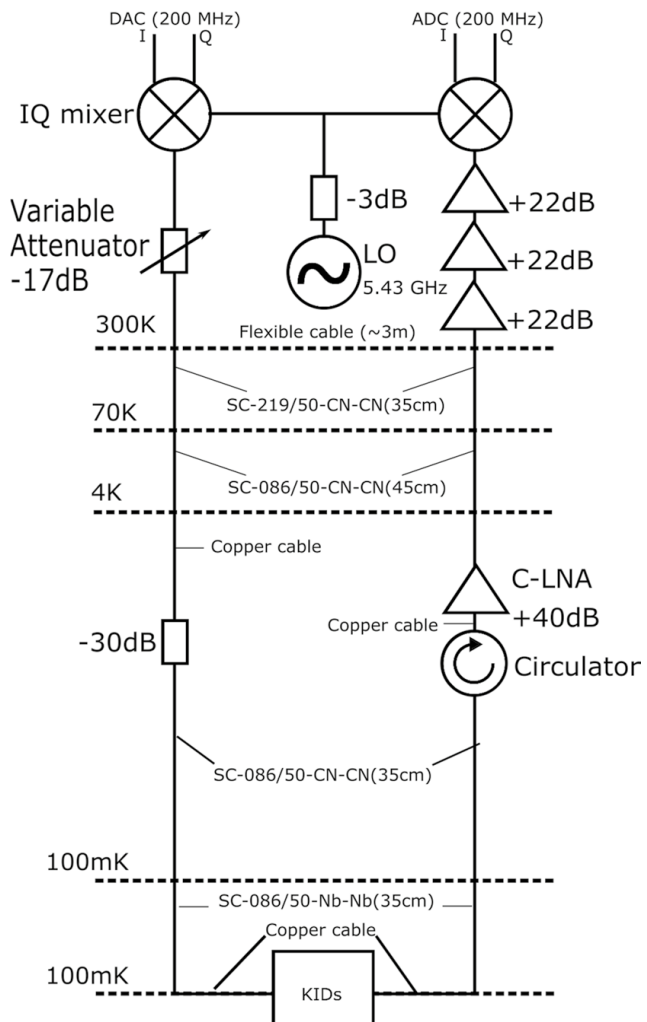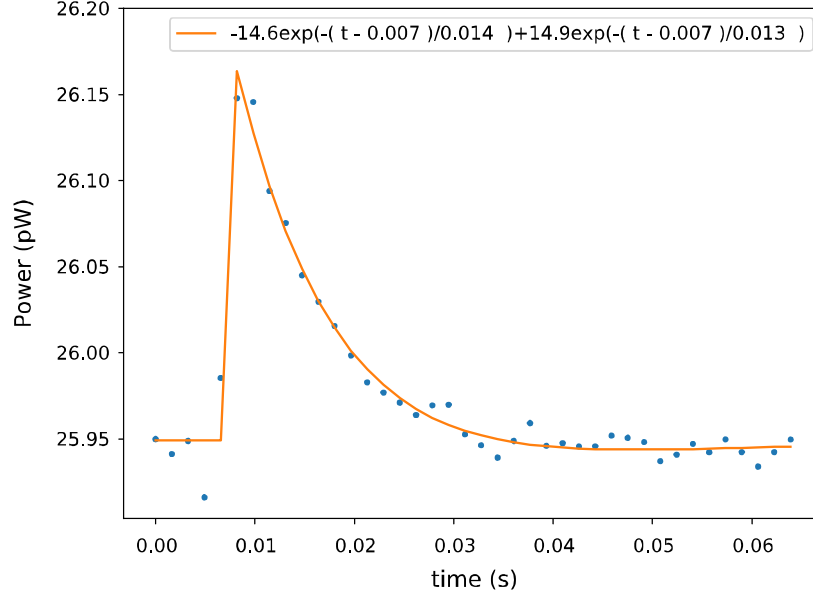
Fig. 6 One example of α-ray hit TOD of "Control Far" TES bolometer. Blue dots show data, and orange line shows the fitted by Eq. (1). Thanks to the first term in Eq. (1), the rising slope is fitted without neglect. And the fitted τ_B is ~ 10 ms and is consistent with our expectation (Color figure online)

3 Results

3.1 Results from TES Bolometers

Because we have unsolved issues, we report the results with two TES bolometers: "Control Far" and "Palladium Far".

We take about 5 h of time-ordered data (TOD) of the two bolometers. For the triggering data, we use mean ($\langle d \rangle$) and standard deviation (σ) with every 30 min of TOD. We prepare a trigger which requires four consecutive data ($(d_i - \langle d \rangle)/\sigma$) to excess threshold of [5, 3, 3, 3]. Then, triggered data are fitted by Eq. (1) as shown in Fig. 6. All signals of two TES bolometers are fitted, and the fitted parameters are shown in Figs. 7 and 8.

From Fig. 7, we see that signal rate for "Palladium Far" is smaller that that of "Control Far". From Fig. 8, we see that most of events show $A \sim B$. This agrees with our assumption that $A \sim B$ if energy deposited to silicon substrate. In usual analysis, the first term in Eq. (1) is neglected. However, as shown in Fig. 6, the first term helps to fit the rising shape of a glitch.

3.2 Results from KIDs

We took time-ordered data (TOD) of amplitudes at resonant frequency for all KIDs. If a phonon interacts with a KID, the phonon breaks a Cooper pair. Electrons from the Cooper pair change the inductance of the KID, changing the
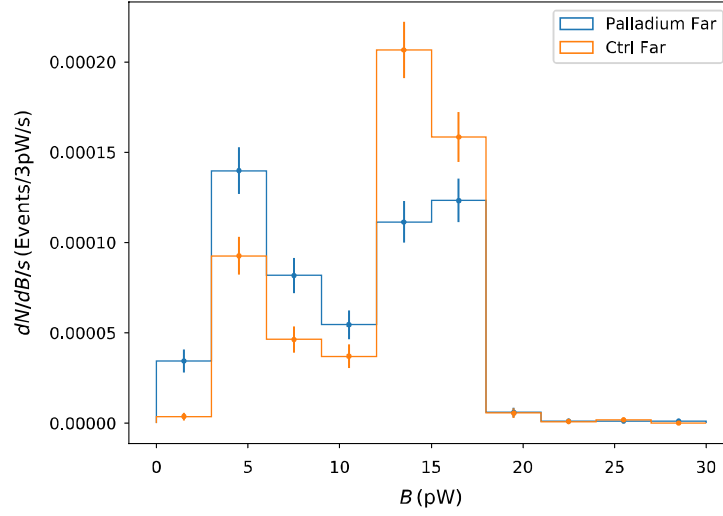
Fig. 7 Histograms of amplitude of signal, "B", fitted by Eq. (1). Histogram is normalised by integrated time (Color figure online)
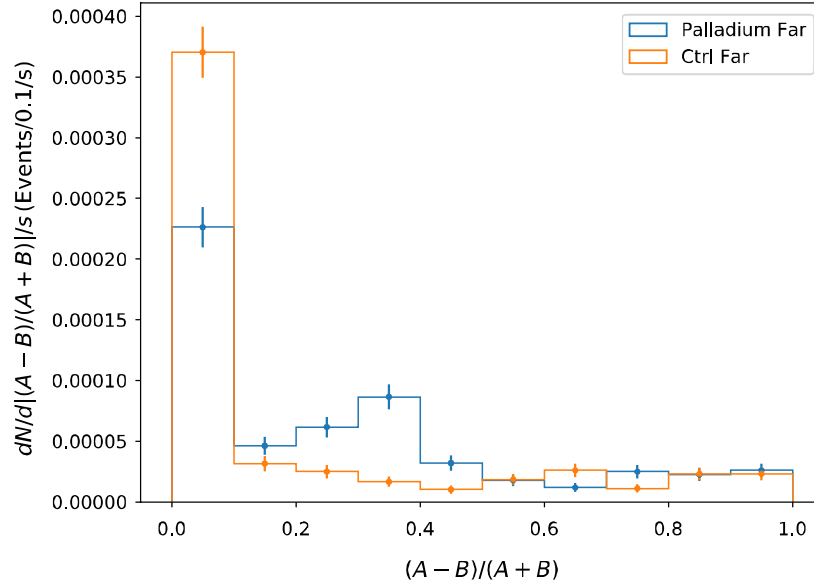
Fig. 8 Histograms of difference of two amplitude, "$|A - B|/(A + B)$", fitted by Eq. (1). Histogram is normalised by integrated time (Color figure online)

Table 2 Summary of modules used in KIDs readout system

Components	Description
HEMT amplifier	NF-LNC4/8C (Low noise factory)
Local oscillator (LO)	e8257d (Keysight)
Splitter	ZFSC-2-9G-S+ (Mini-Circuits)
Variable attenuator	LDA-602 (Vaunix)
IQ mixer	MLIQ-0218L (Marki)
Isolator	QCI-060400C000 (QUINSTAR technology)
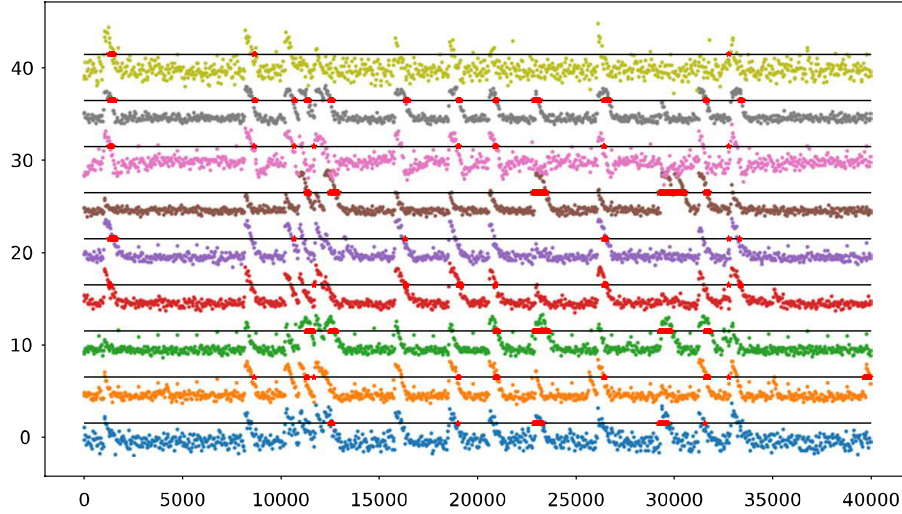
Fig. 9 40 ms TOD of KIDs. The signal height is normalised by $(d_i - \langle d \rangle)/\sigma_d + N \times 5$, where N is the numbering of a KID (f_N). Black lines correspond to threshold for trigger (1.5σ). Red dots show triggered data points (Color figure online)

resonant frequency. Therefore, if we see a change in amplitude at the resonant frequency, we see that a phonon has entered the KID.

We take 10 min of TOD with sampling rate of 25 kSPS. In actual data taking, we take 1000 data points per file (40 ms per file). We calculate mean ($\langle d \rangle$) and standard deviation (σ_d) from all data points (d_i) per one file.

Because we only saw the nine out of the ten KIDs, as an initial step, we identified one dropped KID with the procedure described in Appendix 2.

To pick up phonon events, a trigger is created with three consecutive data points which have $(d_i - \langle d \rangle)/\sigma_d > 1.5$, where d_i is the ith data point, and $\langle d \rangle$ and σ_d are the mean and standard deviation of data points in 1000 data points. Then, we labelled the sampling time index (t_j) with $j \in [i-2, i+5]$ as times with triggered events. The example TOD is shown in Fig. 9. It shows many hit events and a strong correlation between all KIDs. This can be explained by that charged particles hit the ground plane of the KID and change the resonances of all the KIDs. To remove the strong correlation, we applied a veto for the correlation analysis. We require the number of triggered KIDs to be less than six. After the veto, we make a correlation analysis.

We take correlations of diagonally opposite KID pairs across the Control/Hole/Metal area. Because we are concerned about the case that α-ray hit itself is reduced by Hole/Metal area between KIDs, we require prior triggers for the correlation analysis. For example, to see the metal effects, we require trigger with f6 and f4 and calculate correlation between f4 and f10. The other cases and resulted correlations are summarised in Table 3.

It shows that correlation targeting to evaluate "Metal" method shows coincidences compared to the correlation targeting to evaluate "Control". However, concerning the "Hole" method, the correlation is comparable with or slightly smaller than "Control".

Table 3 Summary of correlation analysis with KIDs	Target	Triggering	Combination	Correlation
	Control	f5 and f7	f7 and f2	0.712 ± 0.039
		f6 and f4	f4 and f9	0.534 ± 0.025
	Hole	f5 and f3	f3 and f9	0.57 ± 0.18
	Metal	f6 and f4	f4 and f10	0.32 ± 0.11
		f6 and f8	f8 and f2	0.37 ± 0.11

4 Discussion and Conclusions

From analysis of TES bolometers, we show that putting metal on the silicon substrate can reduce the event rate of α-ray hits on the substrate. We also show that the events with $A \sim B$ are the case where charged particles hit the silicon substrate.

From analysis of KIDs, we show that putting metal reduces the heat propagation.

Because we only see two bolometers, analysis with more TES bolometers remains as a future work. For the future works in the measurements with KIDs: (1) when charged particles deposit energy in the ground plane, all KIDs show a strong correlation. To reduce this effect, irradiation from the backside is preferable. (2) Because we have dropped KIDs, we can have a better analysis with all ten KIDs.

Overall, collimating the α-ray can help to better understand the phonon propagation.

Appendix 1: Modelling of a TES Bolometer

From the model of Fig. 2, we created simultaneous differential equations of temperatures of a TES bolometer and a silicon substrate:

$$\frac{\mathrm{d}}{\mathrm{d}t} \begin{pmatrix} \Delta T_1(t) \\ \Delta T_2(t) \end{pmatrix} = \begin{pmatrix} -\frac{G_1+G_2}{C_1} & \frac{G_2}{C_1} \\ \frac{G_2}{C_2} & -\frac{G_2}{C_2} \end{pmatrix} \begin{pmatrix} \Delta T_1(t) \\ \Delta T_2(t) \end{pmatrix} \quad (2)$$

$$\begin{pmatrix} \Delta T_1(t) \\ \Delta T_2(t) \end{pmatrix} = \alpha_1 \begin{pmatrix} \frac{G_2}{C_1} \\ \Lambda_1 \end{pmatrix} e^{\lambda_1 t} + \alpha_2 \begin{pmatrix} \frac{G_2}{C_1} \\ \Lambda_2 \end{pmatrix} e^{\lambda_2 t}, \quad (3)$$

where ΔT_1 and ΔT_2 are change in temperature of silicon substrate and TES bolometer, $\Lambda_{1,2} = \lambda_{1,2} + \frac{G_1+G_2}{C_1}$,

$$\lambda_1 = -\frac{1}{2}\left[\frac{G_1 + G_2}{C_1} + \frac{G_2}{C_2} + \sqrt{D}\right]$$

$$\lambda_2 = -\frac{1}{2}\left[\frac{G_1 + G_2}{C_1} + \frac{G_2}{C_2} - \sqrt{D}\right],$$

(4)

and

$$D = \left(\frac{G_1 + G_2}{C_1} + \frac{G_2}{C_2}\right)^2 - 4\frac{G_1 G_2}{C_1 C_2}.$$

(5)

If we consider an initial state that the energy (E_{in}) is injected into a silicon substrate at t_0,

$$\Delta T_2(t) = \frac{1}{\lambda_2 - \lambda_1}\Lambda_1\Lambda_2\frac{E_{\text{in}}}{G_2}\left(e^{\lambda_1(t-t_0)} - e^{\lambda_2(t-t_0)}\right)$$

(6)

If we consider an initial state that the energy (E_{in}) is injected into a TES bolometer at t_0,

$$\Delta T_2(t) = \frac{E_{\text{in}}}{C_2(\lambda_2 - \lambda_1)}\left(-\Lambda_1 e^{\lambda_1(t-t_0)} + \Lambda_2 e^{\lambda_2(t-t_0)}\right)$$

(7)

Appendix 2: Finding Dropped KID

Because we only have nine resonances out of ten designed KIDs, we develop a way to identify one dropped KID. For this analysis, we apply the same veto as described in Sec3.2.

After the veto, we calculate the correlation between ith and jth KIDs with triggered time index from ith KID, Corr($d_i(t_i), d_j(t_i)$). This means that Corr($d_i(t_i), d_j(t_i)$) and Corr($d_j(t_j), d_i(t_j)$) are different. Then, we calculate all the correlations between all bolometers. The correlations without $f1$ are plotted in Fig. 10. We checked all the cases with correlation plots and finally find $f1$ KID is dropped. As shown in Fig. 10, f2, f4, f7, and f9 have strong correlations as we expect from the design 4.
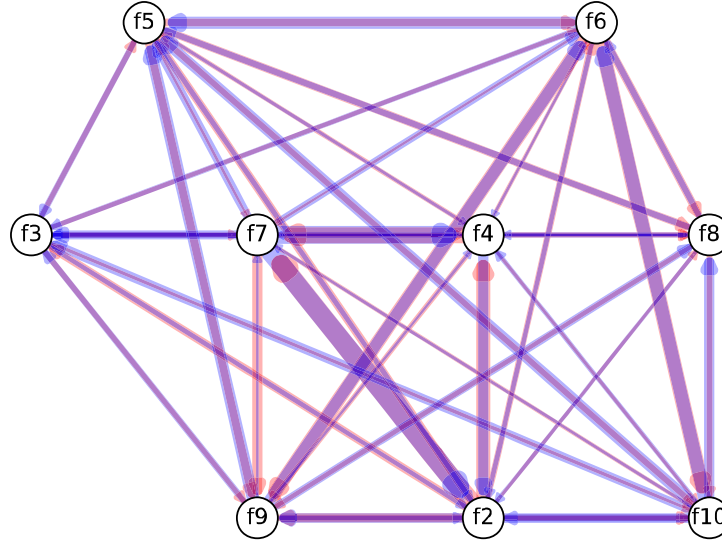
Fig. 10 Digraphs of correlations between KIDs. The vector from *fi* to *fj* shows the correlation of Corr($d_i(t_i), d_j(t_i)$). The red vector shows the case that $i \leq j$, and the blue vector shows the other case. The width of vectors is related to $\propto 1.3 \times 5.0^{\mathrm{Corr}/0.5}$ (Color figure online)

References

1. M. Hazumi et al., Litebird: a satellite for the studies of b-mode polarization and inflation from cosmic background radiation detection. J. Low Temp. Phys. **194**(5), 443–452 (2019). https://doi.org/10.1007/s10909-019-02150-5. ISSN 1573-7357

2. K.D. Irwin, G.C. Hilton, *Transition-Edge Sensors* (Springer, Berlin, 2005), pp. 63–150. https://doi.org/10.1007/10933596_3. ISBN 978-3-540-31478-3

3. Planck HFI Core Team, Planck early results VI The high frequency instrument data processing. Astronomy & Astrophysics **536**, A6 (2011). https://doi.org/10.1051/0004-6361/201116462

4. D. Brandt et al., Monte Carlo simulation of massive absorbers for cryogenic calorimeters. J. Low. Temp. Phys. **167**, 485–490 (2012). https://doi.org/10.1007/s10909-012-0480-3

5. D. Brandt et al. Semiconductor phonon and charge transport Monte Carlo simulation using Geant4. arXiv: 1403.4984 (2014)

6. E. Bagli, M. Asai, D. Brandt, A. Dotti, V. Guidi, D.H. Wright, A model for the interaction of high-energy particles in straight and bent crystals implemented in Geant4. Eur. Phys. J. C **74**(8), 2996 (2014). https://doi.org/10.1140/epjc/s10052-014-2996-y

7. H. Ishitsuka, M. Ikeno, S. Oguri, O. Tajima, N. Tomita, T. Uchida, Front-end electronics for the array readout of a microwave kinetic inductance detector towards observation of cosmic microwave background polarization. J. Low Temp. Phys. **184**(1), 424–430 (2016). https://doi.org/10.1007/s10909-015-1467-7. ISSN 1573-7357

8. J. Suzuki, H. Ishitsuka, K. Lee, S. Oguri, O. Tajima, N. Tomita, E. Won, Development of a data acquisition system for kinetic inductance detectors: wide dynamic range and high sampling rate for astronomical observation. J. Low Temp. Phys. **193**(3), 562–569 (2018). https://doi.org/10.1007/s10909-018-2033-x. ISSN 1573-7357

9. K. Hattori, Y. Akiba, K. Arnold, D. Barron, A.N. Bender, A. Cukierman, T. de Haan, M. Dobbs, T. Elleflot, M. Hasegawa, M. Hazumi, W. Holzapfel, Y. Hori, B. Keating, A. Kusaka, A. Lee, J. Montgomery, K. Rotermund, I. Shirley, A. Suzuki, N. Whitehorn, Development of readout electronics for polarbear-2 cosmic microwave background experiment. J. Low Temp. Phys. **184**(1), 512–518 (2016). https://doi.org/10.1007/s10909-015-1448-x. ISSN 1573-7357

10. A. Suzuki, K. Arnold, J. Edwards, G. Engargiola, A. Ghribi, W. Holzapfel, A.T. Lee, X.F. Meng, M.J. Myers, R. O'Brient, E. Quealy, G. Rebeiz, P. Richards, D. Rosen, P. Siritanasak. Multichroic dual-polarization bolometric detectors for studies of the cosmic microwave background, in *Millimeter, Submillimeter, and Far-Infrared Detectors and Instrumentation for Astronomy VI*, vol. 8452,

ed. by W.S. Holland (International Society for Optics and Photonics, SPIE, 2012), pp. 1038–1047. https://doi.org/10.1117/12.924869

Affiliations

Y. Minami[1] ⬤ · Y. Akiba[1,2] · S. Beckman[3] · M. Hazumi[1,2,4,5] · C. Kuo[6,7] · N. A. Kurinsky[8,9] · H. Kutsuma[10,11] · A. T. Lee[3,12] · S. Mima[11] · C. R. Raum[3] · T. Sasse[3] · S. L. Stever[5] · A. Suzuki[12] · B. Westbrook[3]

[1]   High Energy Accelerator Research Organization (KEK), Tsukuba, Ibaraki 305-0801, Japan

[2]   The Graduate University for Advanced Studies (SOKENDAI), Miura District, Hayama, Kanagawa 240-0115, Japan

[3]   Department of Physics, University of California, Berkeley, CA 94720, USA

[4]   Institute of Space and Astronautical Science (ISAS), Japan Aerospace Exploration Agency (JAXA), Sagamihara, Kanagawa 252-5210, Japan

[5]   Kavli Institute for the Physics and Mathematics of the Universe (Kavli IPMU, WPI), UTIAS, The University of Tokyo, Kashiwa, Chiba 277-8583, Japan

[6]   Department of Physics, Stanford University, Stanford, CA 94305-4060, USA

[7]   SLAC National Accelerator Laboratory, Kavli Institute for Particle Astrophysics and Cosmology (KIPAC), Menlo Park, CA 94025, USA

[8]   Fermi National Accelerator Laboratory, Batavia, IL 60510, USA

[9]   Kavli Institute for Cosmological Physics, University of Chicago, Chicago, IL 60637, USA

[10]   Astronomical Institute, Tohoku University, 6-3 Aramaki, Aoba-ku, Sendai 980-8578, Japan

[11]   RIKEN Center for Advanced Photonics, 2-1 Hirosawa, Wako 351-0198, Japan

[12]   Physics Division, Lawrence Berkeley National Laboratory, Berkeley, CA 94720, USA